Electronic coherences built by an attopulse control the forces on the nuclei

Manuel Cardosa-Gutierrez[1], R. D. Levine[2,3,4], F. Remacle[1,2*]

[1]Theoretical Physical Chemistry, UR MOLSYS, University of Liege, Belgium
[2]Fritz Haber Center, Institute of Chemistry, The Hebrew University of Jerusalem, Jerusalem 91904, Israel
[3] Department of Molecular and Medical Pharmacology, David Geffen School of Medicine and
[4] Department of Chemistry and Biochemistry, University of California, Los Angeles, CA 90095, USA

Abstract

Attopulses have an energy bandwidth broad enough to coherently excite several electronic states of molecules. Towards the control of chemical reactivity by attopulses we derive the quantum mechanical expression for the force exerted on the nuclei in such a vibronic wave packet both during and after the exciting pulse. Tuning the pulse parameters allows accessing specific electronic coherences that determine the force strength and direction during and after the pulse. Following the pulse, the force due to the non adiabatic interactions accelerates or slows down the motion of the vibronic wave packet on the excited electronic states and its sign controls the direction of population transfer. Computational results for the LiH and LiT molecules and the probing by the emission dipole are discussed.

* Corresponding author email fremacle@uliege.be

1. Introduction

Electronic coherences arise in molecules when wave packets on two different electronic states overlap. Broad-in-energy attosecond pulses[1-3] allow exciting coherently several electronic states in molecules, thereby creating electronic coherences in the Franck-Condon region. These electronic coherences drive the motion of the non-equilibrium electronic density on a purely electronic time scale, before a significant onset of the nuclear motion.[4-7] They induce ultrafast charge migration between different parts of the molecule during which one could implement charge directed reactivity.[8-12] In molecules excited by attopulses, the vibronic dynamics is therefore in a post Born-Oppenheimer regime[13]. The electronic state is not in equilibrium with the instantaneous position of the nuclei and so can be exploited to control chemical reactivity.[14-18] Tuning the parameters of the pulse, such as its carrier frequency, envelope duration, polarization and carrier envelope phase (CEP) provides control of the electronic motion in the initially pumped state and of the entanglement between the electronic and nuclear motions.[19-21] Towards this goal, we discuss here the relative importance of the different terms of the exact quantum mechanical force exerted by the vibronic wave packet on the nuclei during and after the pulse. As a practical example, we use fully quantum dynamical simulations of the response of the LiH molecule to ultra short IR and DUV (Deep UV, with carrier frequencies in the range $\approx$ 4-6 eV) pulses that allow controlling the subsequent dynamics.[15, 17, 18, 22, 23] To further examine the force, we compare the dynamics in the LiH and its LiT isotopomer, T=^{3}H, and compute the emission dipole, whose time dependence tracks the force.

2. Quantum mechanical force exerted by a vibronic wavepacket

2.1 The four terms of the quantum mechanical force

The force exerted by the vibronic wave packet on the nuclei is defined as the time-derivative of the mean value of the nuclear momentum, for a diatomic molecule, $\hat{P}_N = -i\hbar\hat{\nabla}_R$, over the vibronic wave function. The vibronic wave function is expanded in a basis of separable terms, $\phi_n^{el}(\mathbf{r};R)\chi_n(t,R)$,

$$\left|\Psi(t,\mathbf{r},R)\right\rangle = \sum_n \phi_n^{el}(\mathbf{r};R)\chi_n(t,R) \tag{1}$$

where $\mathbf{r}$ stands for the electronic coordinates and R the internuclear distance. The electronic wave functions $\phi_n^{el}(\mathbf{r};R)$'s are the adiabatic electronic states, $\hat{H}^{el}\phi_n^{el}(\mathbf{r};R) = E_n(R)\phi_n^{el}(\mathbf{r};R)$, and $\chi_n(t,R)$ is the time-dependent nuclear wave function. Using the Ehrenfest theorem (atomic units (a.u.) are used throughout), one gets for the force:

$$F_{tot} = \frac{d\langle \hat{P}_N \rangle}{dt} = i\left\langle \left[\hat{P}_N, \hat{H} \right] \right\rangle = -\left\langle \left[\hat{\nabla}_R, \hat{H} \right] \right\rangle \tag{2}$$

The full Hamiltonian, $\hat{H} = \hat{T}_N + \hat{H}^{el} - \mathbf{E}(t).\hat{\boldsymbol{\mu}}$, includes the interaction of the molecule with the electric field, $\mathbf{E}(t)$, of the pulse in the dipole approximation, $\hat{\boldsymbol{\mu}}$ is the molecular dipole. Note that in general, the polarization direction of the electric field can make an angle with respect to the molecular axis of the diatomic molecule.[15] In the examples below, we consider oriented LiH molecules for which the polarization direction is parallel to the internuclear axis. Computing the commutators and integrating over electronic coordinates, the total force is a sum of four terms:

$$F_{tot} = -\left\langle \left(\hat{\nabla}_R V(R) \right) \right\rangle + \left\langle \left[\hat{\tau}, V(R) \right] \right\rangle + \mathbf{E}(t) \cdot \left\langle \left(\hat{\nabla}_R \mu(R) \right) \right\rangle - \mathbf{E}(t) \cdot \left\langle \left[\hat{\tau}, \mu(R) \right] \right\rangle \tag{3}$$

where $V(R)$ is the potential energy and $\hat{\tau}$ is the non adiabatic coupling (NAC) between the electronic states, $\tau_{nm} = \left\langle \phi_n^{el} \middle| \hat{\nabla}_R \middle| \phi_m^{el} \right\rangle$. The first two terms of Eq. (3) were derived by F. T. Smith[24] thereby defining a generalized momentum, $\hat{\mathcal{P}} = \hat{P}_N + \hat{\tau}$, see also [25, 26]. The third and fourth terms are due to the interaction with the light field. Their introduction and their role in control are the central subjects of this paper.

The force defined in Eq. (3) is an average over both electronic and nuclear degrees of freedom both of which are treated quantum mechanically. It is the instantaneous force on the nuclei and, as such, it is different from the mean field force for the motion of the classical nuclei derived in Ehrenfest dynamics, which is obtained by averaging over the electronic wave functions, ϕ_n^{el} 's, only [27-29].

2.2 Explicit expressions for the quantum dynamics of a diatomic molecule

The vibronic dynamics in LiH is computed for several coupled electronic states using a grid description for the internuclear distance as in previous works[17, 30]. The vibronic wave function is written as

$$\left| \Psi(t) \right\rangle = \sum_{g=1}^{N_g} \sum_{i=1}^{N_e} c_{gi}(t) \left| gi \right\rangle \tag{4}$$

where $\left| gi \right\rangle$ is a basis function localized at grid point g on the adiabatic electronic state i. In the results reported below, we include N_g=512 grid points and $N_e = 7$ electronic states. The molecular Hamiltonian, $\mathbf{H}$, used to integrate the time-dependent Schrödinger equation,

3

$d\mathbf{c}/dt = -i\mathbf{H}\mathbf{c}$, includes all the NAC terms and the interaction with the pulse in the dipole approximation. For a diatomic molecule, we get

$$\mathbf{H} = \boldsymbol{\mathcal{P}}^2 + V(R) - \mathbf{E}(t)\cdot\boldsymbol{\mu}$$
$$= -\frac{1}{2\mu}\left(\nabla_R^2 + 2\boldsymbol{\tau}(R).\nabla_R + \left(\nabla_R\boldsymbol{\tau}(R)\right) + \boldsymbol{\tau}(R).\boldsymbol{\tau}(R)\right) + V(R) - \mathbf{E}(t).\left(\boldsymbol{\mu}^{nuc}(R) + \boldsymbol{\mu}^{el}(R)\right) \quad (5)$$

Where

$$\boldsymbol{\mu} = \boldsymbol{\mu}^{nuc}(R) + \boldsymbol{\mu}^{ele}(R) \quad (6)$$

The electronic dipole, $\mu^{el}(R)$, is diagonal in grid points

$$\boldsymbol{\mu}^{el}(R) = \sum_{i,j=1}^{N_e} \boldsymbol{\mu}_{ij}^{el}(R) \quad (7)$$

The nuclear dipole is given by

$$\boldsymbol{\mu}^{nuc}(R) = \sum_{\alpha=1}^{N_{nuc}} eZ_\alpha R_\alpha = f\, R, \quad f = \left(m_H Z_{Li} - m_{Li} Z_H\right)/\left(m_{Li} + m_H\right) = 0.5 \quad (8)$$

in the molecular frame attached to the center mass, where the Li has a positive z coordinate, see Figure S1. The explicit expression of the force (Eq. (3)) in terms of the vector of the time-dependent amplitudes, $\mathbf{c}$ (Eq. (4)), takes the form:

$$F_{tot} = -\mathbf{c}^T\left(\nabla_R V\right)\mathbf{c} - \mathbf{c}^T\left[\boldsymbol{\tau},\mathbf{V}\right]\mathbf{c}$$
$$+\mathbf{E}(t)\cdot\left(\mathbf{c}^T\left(\nabla_R\boldsymbol{\mu}^{nuc}\right)\mathbf{c} + \mathbf{c}^T\left(\nabla_R\boldsymbol{\mu}^{el}\right)\mathbf{c}\right) + \mathbf{E}(t)\cdot\left(\mathbf{c}^T\left[\boldsymbol{\tau},\boldsymbol{\mu}^{el}\right]\mathbf{c}\right) \quad (9)$$

In principle it is clear from equation (9) but in view of its importance we point out explicitly that in addition to terms diagonal in the electronic index of the states there is also significant contributions from the coherences between different elecronic states. The control of these coherences is an essential part of our ability to control the force.

In equation (9) the third and fourth terms gather all the contributions to the force that result from the dipole interaction and can be controlled by the pulse parameters:

$$F_{dip} = +\mathbf{E}(t)\left(\mathbf{c}^T\left(\nabla_R\boldsymbol{\mu}^{nuc}\right)\mathbf{c} + \mathbf{c}^T\left(\nabla_R\boldsymbol{\mu}^{el}\right)\mathbf{c}\right) + \mathbf{E}(t)\left(\mathbf{c}^T\left[\boldsymbol{\tau},\boldsymbol{\mu}^{el}\right]\mathbf{c}\right) = F_\mu + F_{[\tau,\mu^{el}]} \quad (10)$$

where

$$F_\mu = E(t)\sum_{gi}\left|c_{gi}(t)\right|^2\left(\left(\nabla_R\mu_g^{nuc}\right) + \left(\nabla_R\boldsymbol{\mu}_{gi,gi}^{ele}\right)\right) + \sum_{gi,gj,j\neq i} c_{gi}(t)c_{gj}^*(t)\left(\nabla_R\boldsymbol{\mu}_{gi,gj}^{ele}\right) \quad (11)$$

and depends on the electronic coherences through its second term. $\mu^{nucl}(R)$ has a linear dependence with respect to R (Eq. (8)), so that $\mathbf{E}(t)\sum_{gi}\left|c_{gi}(t)\right|^2\nabla_R\mu_g^{nuc} = 0.5\,\mathbf{E}(t)$ and the

nuclear dipole $\boldsymbol{\mu}^{nuc}$ does not contribute to the commutator $\left[\boldsymbol{\tau},\boldsymbol{\mu}\right]$. The term $F_{\left[\tau,\mu^{ele}\right]}$ also depends on the electronic cooherences

$$F_{\left[\tau,\mu^{el}\right]} = \mathbf{E}(t)\sum_{i,j,k}^{Ne}\sum_{g}^{Ng} c_{gi}^*(t)c_{gk}(t)\left(\tau_{gi,gj}\mu_{gj,gk}^{el} - \mu_{gi,gj}^{el}\tau_{gj,gk}\right) \qquad (12)$$

The first two terms of Eq. (9) depend on the potentials $V(R)$ of the electronic states

$$F_{pot} = -\mathbf{c}^T\left(\nabla_R V\right)\mathbf{c} - \mathbf{c}^T\left[\boldsymbol{\tau},\mathbf{V}\right]\mathbf{c} = F_V + F_{\left[\tau,V\right]} \qquad (13)$$

$$F_V = \sum_{gi}^{NeNg} \left|c_{gi}\right|^2(t)\nabla_R V_{gi} \qquad (14)$$

$$F_{\left[\tau,V\right]} = \sum_{i,k}^{Ne}\sum_{g}^{Ng} c_{gi}^*(t)c_{gk}(t)\tau_{gi,gk}\left(V_{gk} - V_{gi}\right) \qquad (15)$$

In Eqs (10) and (13), the terms that depend on the gradients, $\nabla_R\mu^{nuc}$ and $\nabla_R V$, are an average over the populations in each electronic state, while the other terms oscillate with the periods of the electronic coherences, $c_{gi}^*(t)c_{gk}(t)$. From Eq. (10) one can anticipate that the force due to the dipole interaction, F_{dip}, can be manipulated by tailoring the magnitude, the time profile and the polarization of the electric field of the pulse, to either counteract or enhance the effect of the potential term, F_{pot} (Eq. (13)).

We illustrate the time-dependence of the force on the nuclei exerted by a fully quantal vibronic wave function both during and after the excitation of the LiH molecule by an attopulse. We show that tuning the force due to the interaction with the pulse electric field, F_{dip} (Eq. (10)), with the attopulse parameters can be effectively applied to control the force on the nuclei for realistic pulses. Two types of control are discussed: a control by one cycle strong NIR pulses that differ by their CEP values and by a several cycle 4 fs VIS pulse. Note that the time dependence of the total force can be computed straighforwardly by taking the numerical derivative of the mean value of the generalized momentum, $d\langle\mathcal{P}\rangle/dt$, with $\hat{\mathcal{P}} = -i\hat{\nabla}_R + \hat{\tau}$.

The quantum dynamics is computed using the potential energy, dipole and NAC curves of ref. [17]. For completeness, they are plotted in Figures S1-S3 of the SM. We take the pulse to be oriented along the molecular axis (see Figure S1 for the orientation of LiH in the molecular frame) which is a reasonable approach because of the large value of the permanent dipole of the LiH molecule, (at equilibrium $\mu_{eq}^{el} = 2.1$ a.u.).[31, 32] By optical selection rules, such a pulse

5

excites the manifold of Σ states only. The pulse is defined by $\mathbf{E}(t) = -d\mathbf{A}(t)/dt$ and the vector potential $\mathbf{A}(t)$ has a Gaussian envelope:

$$\mathbf{E}(t) = \mathbf{E}_0 \cdot \exp\left(-(t-t_p)^2/2\sigma_p^2\right)\left[\cos\left(\omega_p(t-t_p)\right) - \left(\frac{t-t_p}{\omega_p\sigma_p^2}\right)\sin\left(\omega_p(t-t_p)\right)\right] \quad (16)$$

3. Results and discussion

We begin by a NIR essentially one cycle pulse, with a carrier frequency of $\omega = 0.0633$ a.u. (720 nm), a FWHM = 0.8 fs, centered at 12.1 fs (500 a.u.) and a peak intensity of 0.04 a.u.. Here the relevant control parameter is the value of the CEP. A CEP = 0 corresponds to the maximum of $\mathbf{E}(t)$ oriented towards the Li atom while a CEP = π corresponds to the maximum of $\mathbf{E}(t)$ oriented towards the H atom, see Fig. S1 of the SM. The populations in the electronic states of the LiH molecule during this pulse are plotted in Figure 1 a and b for the two CEP's. As discussed previously,[15, 18, 33] for oriented LiH molecules, the CEP of the one cycle IR pulse allows selecting which electronic states are preferentially excited because they have alternating sign of their polarity in the FC region. For the pulse used here, a CEP = 0 favors the excitation of the S4 state (Fig. 1a) with lower populations in S2 and S3 while for the CEP = π pulse, the largest population after the pulse is in S1 (Fig. 1b) and the population in S2 is larger than in S3 and S4. The CEP therefore allows controlling the population in the excited states, whose asymptotic populations determine the yields in fragments, each asymptote correlating to a different excited state of the Li atom see Figure S4 of the SM. The total force (Eq.(9)) during the pulse is plotted in Figs. 1 c and d. At its maximum, the force is positive for a CEP = 0, while it is negative for the CEP = π pulse. However, at the maximum of the pulse, the total force (positive) for CEP = 0 (Fig. 1c) is significantly smaller than the force for the CEP = π pulse (Fig. 1d), which is large and negative (-0.04 a.u., one a.u. of force = 82 nN).

This can be understood by analyzing the time dependence and the phase of the different terms contributing to the force, shown in Figs. 1e and f. During the pulse, the term F_V, Eq. (14), due to the potential gradients, remains small for both excitations and the force terms due to the interaction with the pulse, F_{dip} (Eq. (10)) dominate. The force due to the dipole gradient, F_μ, Eq. (11), (blue line in Figs. 1e and f), is dominated by the nuclear dipole contribution (Eq. (11)), the electronic contribution being smaller and of opposite sign, and follows the sign of the electric field. The terms that involve the NAC coupling and the electronic coherences, $F_{[\tau,\mu^{el}]}$ (Eq. (12),orange) and $F_{[\tau,V]}$ (Eq. (15), violet) play a key role, and either enhance or counteract

6

the effect of the F_μ term. Note that the $F_{[\tau,\mu^{el}]}$ term is multiplied by the strength of the electric field. The $F_{[\tau,\mu^{el}]}$ term is large and of opposite sign to F_μ for the CEP=0 excitation while the term $F_{[\tau,V]}$ (violet) remains small, which leads to a small value of the total force during the pulse. The situation is opposite for the CEP=Π excitation, which populates the S1. In that case, the $F_{[\tau,\mu^{el}]}$ is small and the $F_{[\tau,V]}$ term is large and of the same sign as F_μ which leads to a large total force at the maximum of the pulse, aligned with the direction of the electric field. The resulting total force at the maximum of the electric field (- 0.04 a.u., one a.u. of force = 82 nN). During the short pulse, there is no significant mass effect and the patterns of the force terms for the LiT are very similar to those of LiH, see Figure S5.
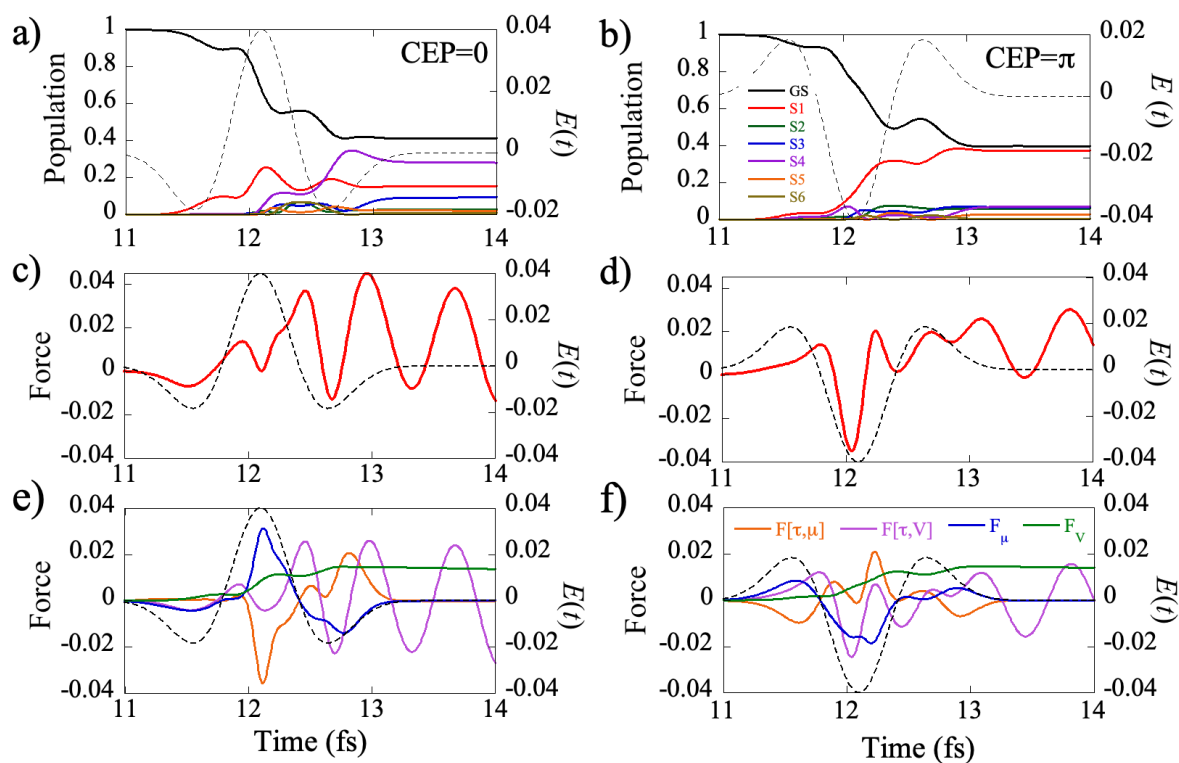

Figure 1. Transient population dynamics during the exciting NIR one cycle pulse a) CEP=0, b) CEP=π . c) and d) time profile of the total force, F_{tot} (Eq.(9)), in red, left ordinate, over the time interval during the pulse, a dashed curve, right ordinate. e) and f) time profile of the four terms of the total force during the pulse (Eqs.(10) to (15)). See figure S5 for the different components of the force for the dynamics in LiT.

The effect of the force on the nuclei can be probed by two dynamical observables, the time-dependence of the emission dipole, and the variation of the mean value of the internuclear distance, $<R(t)>$, as a function of time. We begin by discussing the effect of the force on the mean internuclear distance, $\left\langle R(t)\right\rangle = \sum_{g}^{Ng} \sum_{i}^{N_e} \left| c_{gi}(t) \right|^2 R_g$. Since it does not depend on the electronic index it can be written as an observable on the nuclear density matrix, $\overline{\rho}_{gg'} = \sum_{i=1}^{Ne} c_{gi}^*(t) c_{g'i}(t)$. The ultra short exciting pulse builds a superposition of several electronic states, and the nuclear and electronic motions are correlated throughout the dynamics. Insights on the role of the force on the nuclei exerted by the vibronic wave packet are therefore provided by the projection of $<R(t)>$ on the different electronic states, i, $\left\langle R_i(t) \right\rangle$.

The time dependence of $\left\langle R_i(t) \right\rangle$ on a single bound excited electronic state was reconstructed using pump-probe spectroscopy in the diatomic molecules Na_2[34] and D_2^+[35] monitoring the photoelectron kinetic energy and the kinetic energy of the fragments respectively. $\left\langle R_i(t) \right\rangle$ is recovered from a priori knowledge of the potential curves of the neutral excited state and of the cation for Na_2 and the bound excited state and the dissociative one for D_2^+. These measurements were later related to the nuclear flux[36-38] and extended to the electronic flux[39, 40]. In the case of the excitation by a broad-in energy-short-in-time pulse, several excited electronic are coherently populated and they exchange population because of the non adiabatic coupling, rendering the above flux procedures difficult to implement.

The effect of the sign of the force, in particular of its non classical term, $F_{[\tau,V]}$, on the spreading of the wave packet on the electronic states and on the associated $\left\langle R_i(t) \right\rangle$ values is shown in Figs. 2 and 3. Figure 2 shows the force and the mean value of R, $<R_i(t)>$, for the bound motion on the GS. $<R_{GS}(t)>$ is plotted in fig. 2a and b for the two values of the CEP until the end of the exciting pulse. Also shown in Figure 2 are the time evolution of the only two components of the force which affect $<R_{GS}(t)>$ after the pulse, the term due the gradient, F_{VGS} (Eq.(14)), and the term due to the NAC coupling between the GS and S1, $F_{[\tau,V]GS-S1}$ (Eq.(15)). The internuclear distance, R, is defined as $R = z_{Li} - z_H$ with the origin of the molecular frame attached at the center of mass and $z_{Li} > 0$, see Figure S1. A negative force corresponds to an

elongation of the bond, that is, an increase of R, while a positive force corresponds to a compression of the bond and a decrease of R.

Right after the pulse is over, after 13.5 fs, one can see that the major component of the force is the non classical $F_{[\tau,V]_{GS-S1}}$ term, which is of opposite sign for the two CEP values of the exciting pulse. There is an increase of $<R_{GS}(t)>$ after the pulse for the CEP=0 pulse and a decrease of $<R_{GS}(t)>$ for the CEP=Π. The value of the CEP therefore controls the phase of the vibrational motion on the GS.
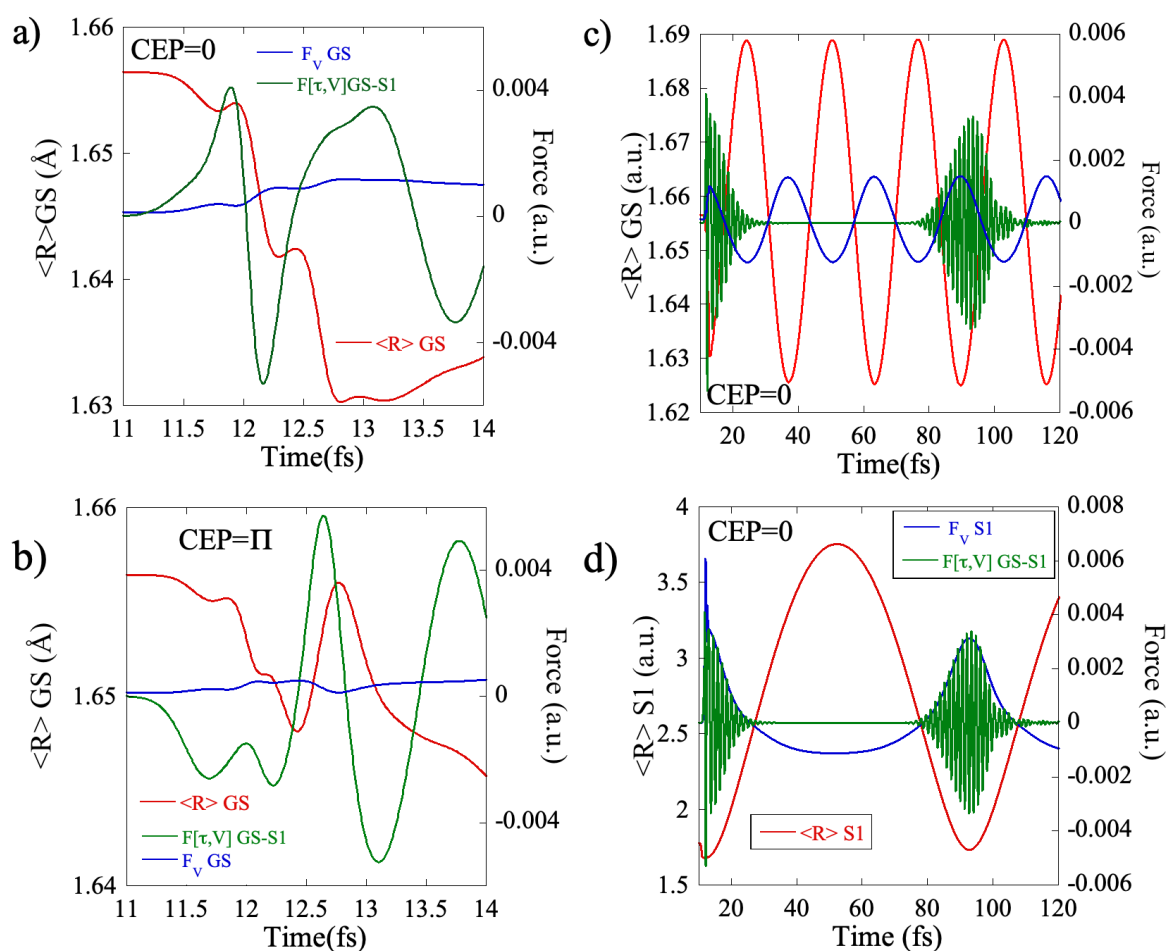
Figure 2. Time evolution of $<R_{GS}(t)>$ and of the two components of the force that control it, F_V (blue) and $F_{[\tau,V]_{GS-S1}}$ (green) during and right after the pulse for the CEP=0 pulse (panel a) and the CEP=Π pulse (panel b). Panels c) and d) long time evolution of the force terms and $<R_{GS}(t)>$ (red) (c) and $<R_{S1}(t)>$ (red) (d) as well as the two components of the force, $F_{[\tau,V]_{GS-S1}}$ and F_V for CEP=0.

At longer times, the electronic coherence GS-S1 vanishes until its revival due to the recurrence of the wave packet on S1 at ≈ 84 fs. So the force for the GS is only due to the potential term, F_V, which leads to oscillations of the bond distance with a period of ≈ 24 fs as shown in Figure 2c for the CEP = 0 pulse. A similar behavior is obtained for the wave packet on S1, shown in Figure 2b, which oscillates with an 84 fs period.

Heatmaps of the localization of the wave packet vs time on the excited electronic states S2, S3 and S4 are plotted in Figure 3. These excited states are dissociative and therefore the contribution of the potential gradient, F_V (black dotted line) to the force becomes negligible after the pulse. Then, the oscillating, non classical $F_{[\tau,V]}$ S2-S3 and S3-S4 terms (blue and green dotted lines) dominate the total force (violet). Their effect is either to slow down or to increase the rate of motion of the wave packet on each potential curve, depending on their sign: a positive sign of the total resulting force decelerates the motion of the wavepacket (and plays the role of a friction term on the considered electronic state) leading to a plateau in $<R_i(t)>$, e.g., Fig.3a around 20 fs. When negative, this term leads to an acceleration of the wavepacket motion, i.e. Fig. 3g around 25 fs. The sign of the $F_{[\tau,V]}$ terms also controls the direction of amplitude transfer, see Figure 6 below and Figure S6.
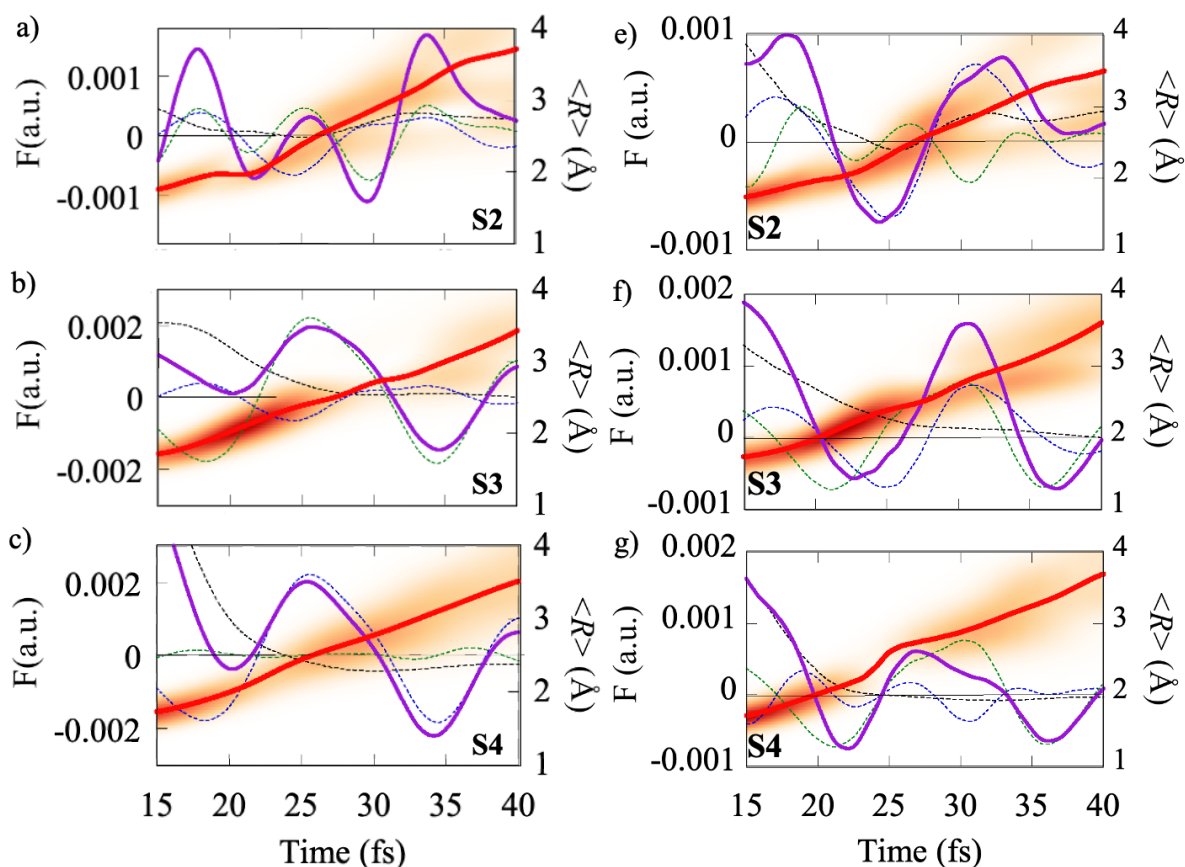
Figure 3: Heatmaps of the time-dependence of localization of the wave packet on the excited electronic states S2, S3 and S4 vs time for the exciting pulse with a CEP=0 (panels a, b, c) and CEP=π (panels e,f,g). $<R_i(t)>$ is plotted in red thick line (right ordinate). The total force affecting the nuclei on electronic state is plotted in thick violet line (left ordinate). Its components are plotted in dotted lines, F_V in black and $F_{[\tau,V]GS-S1}$ for the two states involved in blue and in green.

The effect of the $F_{[\tau,V]}$ terms on the motion of the wave packet on the different electronic states is not limited to one cycle strong NIR pulses of different CEP. It can also be observed in the case of two photon excitation to the S2, S3 and S4 states with a short but several cycle VIS 2.6 eV (476.9 nm) pulse (FWHM 4fs, E_0 = 0.01 a.u.) for which there is no CEP effects and no control through the polarity of the excited electronic states. Here the control is obtained through the carrier frequency and pulse duration. As can be seen from Fig. 3, a significant population transfer occurs through NAC between the S4 state (which is optically bright) and the S3 state (which is darker) during the second half of the pulse, which leads commensurate amounts of

population in the S1, S3 and S4 states at the end of the pulse. S2 is then populated through NAC with S3.
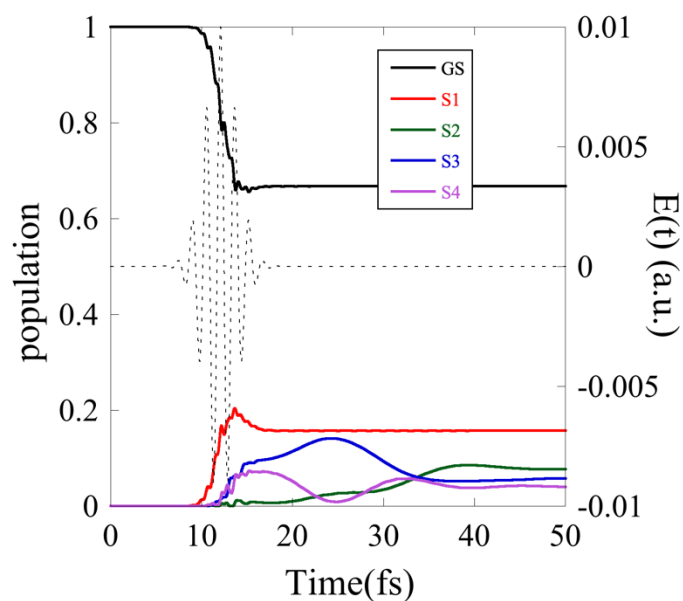

Figure 4. Populations in the excited electronic states resulting from the excitation by a 4fs VIS 2.6 eV pulse (E_0 = 0.01 a.u.). There is no effect of the CEP but tuning the wavelength and the duration of the pulse allows controlling the populations in the excited electronic states. Note how the population in S2 that was essentially zero at the end of the pulse is rising due to the NAC between S3 and S2.

Heatmaps of the localization of the wave packet vs time are shown in Figure 5 for the S2, S3 and S4 states. Here too, one clearly sees that a positive total force (violet) decelerates the motion of the wave packet (in the first 5 fs for all three states) which the wave packet is accelerated by a negative value of the total force. Note that for the excitation by the VIS pulse, the total force in each potential curve are in phase.
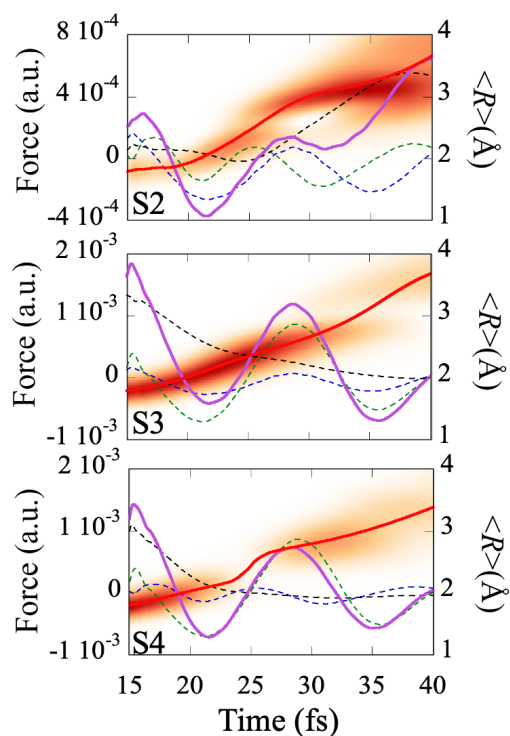
12

Figure 5. Heatmaps of the localization of the wave packet on the excited electronic states S2, S3 and S4 for the exciting pulse VIS pulse of Figure 4. $<R_i(t)>$ is plotted in red thick line. The total force affecting the nuclei in each electronic state is plotted in thick violet line. Its components are plotted in dotted lines, F_V in black and $F_{[\tau,V]}$ for the two states involved in blue and in green.

The key conclusion from the analytical results and the numerical examples discussed above is that the sign of the force also controls the direction of population tranfer. This strengthens the point already made in ref. [41]. Clear additional evidence is provided in Figure 6 that shows the correlation between the population transfer in the excited states and the time-dependence of the force for both the LiH and LiT dynamics induced by the CEP=0 the one cycle NIR pulse in the 15 to 40 fs time interval. For the CEP=0 pulse, the population transfers essentially involve the S3 and S4 states, with the population in S2 slowly increasing in the second half of the time interval. The terms of the force for the S3-S4 interaction, $F_{[\tau,V]}$ S3-S4 (red) and the two potential terms, F_V S3 (blue) and F_V S4 (violet), are plotted in Figures 6 c and d. As discussed for LiH in Figure 3 above, in the regions where the NAC terms are important, the $F_{[\tau,V]}$ S3-S4 term is larger than the F_V terms and oscillates with the period of the S3-S4

13

coherence, $\approx$ 25-20 fs. As indicated by the vertical dotted lines in Figure 6, when $F_{[\tau,V]}$ is negative, that is, when the force leads to an acceleration of the wave packet motion (Figure 3), the population is transferred from S4 to S3. This transfer can be seen in Figure 3 b and c where one can observe a larger localization on S3 than on S4 in the heatmap, as well as in Figure 1a that shows the population dynamics. When $F_{[\tau,V]}$ is positive, the transfer occurs in the opposite direction. The mass difference slows down the motion of the wave packet on the PEC for LiT, leading to a small dephasing in the oscillations of $F_{[\tau,V]}$ (the extrema are delayed with respect to LiH) and a less efficient population transfer in LiT than in LiH between 15 and 25 fs. As the wave packets leave the NAC region, the energy difference between S3 and S4 increases which leads to a shorter period of the electronic coherence. The population transfer patterns for the CEP = π LiH and LiT dynamics as well is the force profiles are more complex because three states, S2, S3 and S4 are involved. They are plotted in Figure S6 of the SM.
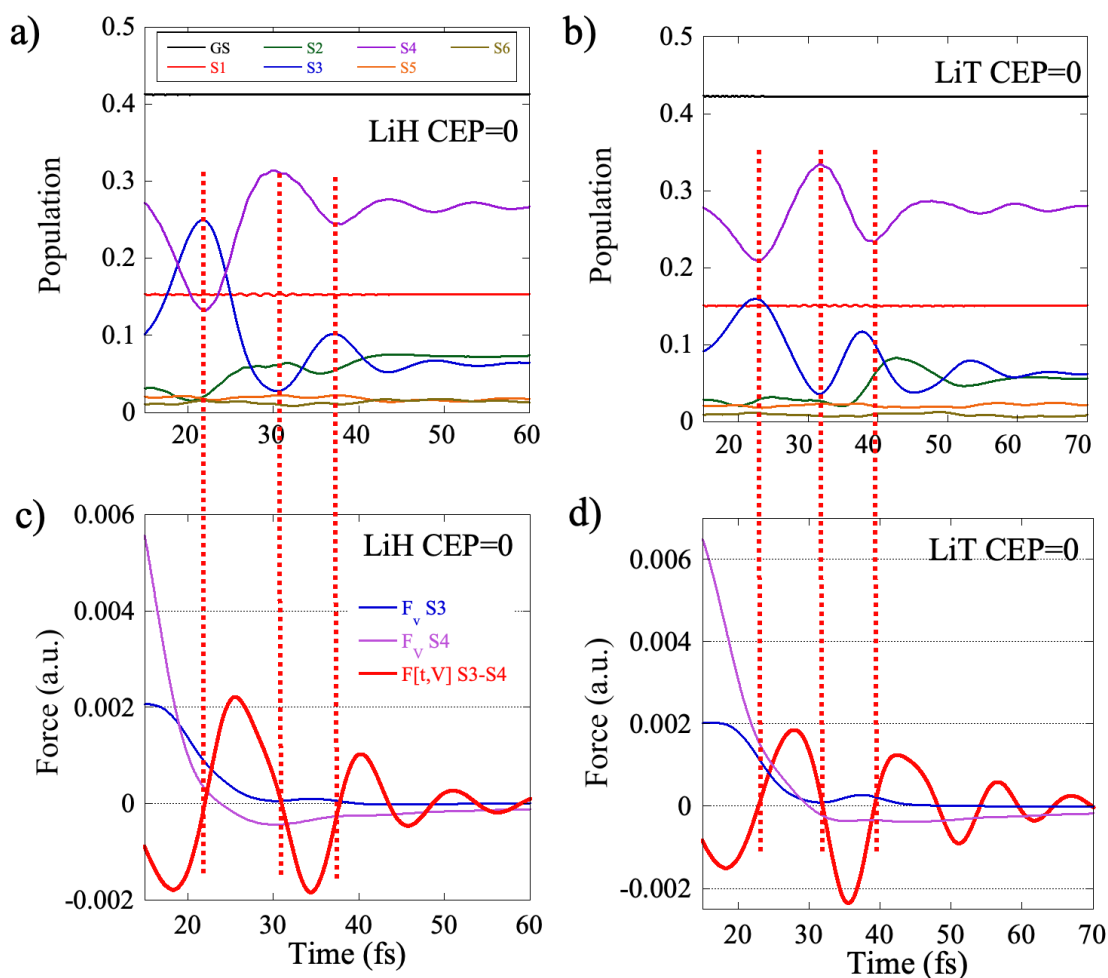
Figure 6: Correlation between the dynamics of population transfers between the S3 and the S4 states for the CEP=0 LiH (panel a) and LiT (panel b) dynamics with the time profile of the force terms (LiH, panel c and LiT, panel d). The vertical dotted lines are drawn at the times when the S3-S4 $F_{[\tau,V]}$ term is zero. When the $F_{[\tau,V]}$ is negative, population is transferred from S4 to S3 and in the reverse direction when it is positive.

As shown in the previous figures, the force terms have complex time profiles and oscillate with both electronic and vibrational periods. Their periods can be directly probed in time by time resolved electric field spectroscopy, a novel kind of time-resolved spectroscopy that provides probing in time of the molecular emission dipole that has been recently developed, [42, 43] or by pump-probe transient absorption spectroscopy[44], see also refs. [16, 18]. The emission dipole is given by the mean value of the dipole, $\hat{\mu}$,

$$\mu(t) = \langle \Psi(t) | \hat{\mu} | \Psi(t) \rangle = f \sum_{gi}^{NgNe} \left| c_{gi}(t) \right|^2 R_g + \sum_{gi,gj}^{NgNe} c_{gi}^*(t) c_{gj}(t) \mu_{gigj}^{el} \qquad (17)$$

It depends on both the electronic and the vibrational coherences as do the terms of the force. As is also the case for the force, the electronic part (second term on the rhs of Eq. (17)) reflects the electron-nuclei correlation. Note that the nuclear part of the dipole (first term on the rhs) is a direct probe of <R(t)> of a diatomic molecule, and that unlike the probing methods discussed above for <R(t)>, the time resolved emitted electric field due to the nuclear dipole is directly proportional to <R(t)> without requiring an a priori knowledge of the potential curves.

We report in Figure 7a the total force and in figure 7b the emitted dipole for the CEP = 0 dynamics in LiH (green) and LiT (red). In both panels and for both isotopomers, one distinguishes short periods of ≈ 1 fs and smaller, that correspond to the electronic transition frequencies between the GS and the excited states and between the S1 state and states S2, S3 and S4 and slower periods of ≈ 20-30 fs that correspond to the transition frequencies between the states of the S2-S3-S4 manifold. On can also distinguish in Figures 7 a and b a much longer period of ≈ 84 fs for LiH and ≈ 124 fs for LiT, which correspond to the vibrational period of the S1 state. When the vibronic wave packet on S1 revisits the FC region after a vibrational period (see Figure 2d), there is revival of the GS-S1 electronic coherence that modulates this recurrence with a faster ≈ 1fs period.

To disentangle the electronic and vibrational periods present in the total force, we show in Figure 7c the Fourier Transform (FT) of the total force computed for the full range of transition frequencies below the IP, from 0 to 8 eV. There are three massifs of peaks in the force power

spectrum, two at high frequencies, at ≈ 3 eV and at ≈ 5- 6 eV and one below 1 eV. The peaks at ≈ 3eV correspond to the electronic transitions GS-S1 and S1 to S2, S3, S4 and the massif at 5-6 eV to the transitions between the GS and the S2-S3-S4 states. Each massif is modulated by vibrational transitions in S1. Similar patterns are obtained for the FT of the dipole moment, see SM, Figure S7. The low frequency range of the force spectrum, below 1eV, corresponds to the vibrational coherences and to the electronic coherences between the states of the S2-S3-S4 manifold which are commensurate. The inset of figure 7c zooms on the low frequency range < 0.5 eV of two the non zero terms of the force after the pulse, F_V and $F_{[\tau,V]}$, plotted in full lines and in dashes respectively. The sharp lines in F_V shift upon isotopic substitution, which can therefore be used to distinguish between electronic and vibratioan periods. They correspond to the vibrational frequencies of the GS (≈25.5 fs, 0.16 eV for LiH and ≈ 38 fs, 0.10 for LiT) and of S1 (≈84 fs, 0.050 eV for LiH and ≈ 124 fs, 0.033 eV for LiT) and their harmonics since a non-stationary vibrational wave packet is formed in these two bound states upon excitation. The fundamentals are the same as those computed by the FT of the total dipole moment of the individual electronic states shown in Figure S8 of the SM and reported in Table S1. The spectrum of the $F_{[\tau,V]}$ term is a broad peak in the range [0.1-0.3] eV common to both isotopomers. It corresponds to the electronic transition frequencies within the S2, S3 and S4 manifold with a weak fine structure, more visible in the case of LiH. The origin of this fine structure can be resolved using gated Fourier Transforms of $F_{[\tau,V]}$ term for specific pairs of states for a short range [15,50] fs and for the full range [15,200] fs of the dynamics after the pulse, see Figures S9 and S10. The fine structure only appears in the long range spectra of the $F_{[\tau,V]}$ terms that involve the S2 state, which is coupled to S1 in the FC region. Figure S11 provides a detailed analysis of the spectra of the $F_{[\tau,V]}$ and the F_V terms computed separately for the S1, S2, S3 and S4 states for the CEP = 0 LiH and CEP = π LiT dynamics.
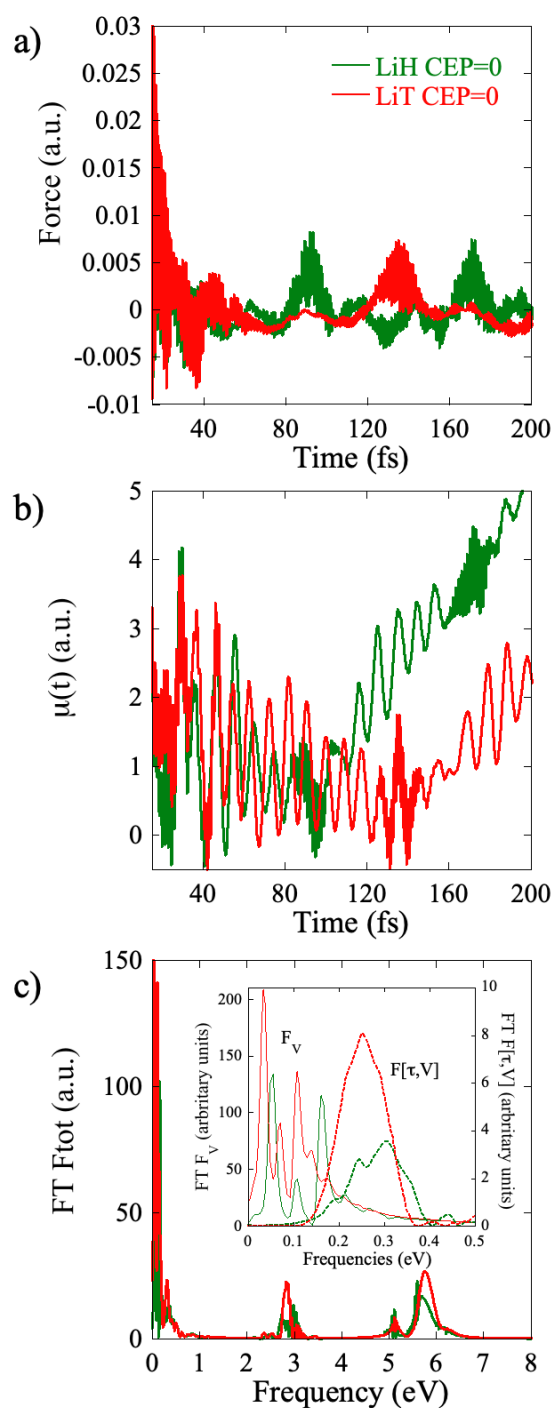
Figure 7 a) The total force, F_{tot} (Eq.(9)), as function of time for the CEP=0 LiH (green) and LiT (red) dynamics. b) The total dipole moment (Eq.(17)) as a function of time.) c) the spectrum of the total force after the pulse as a function of frequency. Inset: the short frequency range of the spectra of the F_V and $F_{[\tau,V]}$ terms that contribute to the total force after the pulse.

17

4. Concluding remarks

We proposed an approach that includes exactly the role of electronically non adiabatic couplings and thereby allows for a detailed analysis of the force exerted by a vibronic wave packet. We presented numerically converged results for the wave packet built by multiphoton excitation of LiH and LiT with broad in energyCEP controlled NIR pulses and a VIS pulse. The total force, Eq.(3), is the sum of four components, two resulting from the dipole interaction that are proportional to the electric field profile, $\mathbf{E}(t)$, of the exciting pulse, F_μ and $F_{\left[\tau,\mu^{el}\right]}$ and two components that depend on the potential, F_V and $F_{\left[\tau,V\right]}$. The second term in either contribution is due to the non adiabatic coupling τ. The terms that depend on the dipole interaction allow tuning the force with the pulse parameters and control the subsequent dynamics. After the pulse, the electronic coherences govern the oscillations of the force term due to the non adiabatic interaction, $F_{\left[\tau,V\right]}$. This force term plays the role of a friction for the motion of the wave packets on the different potential curves and competes with the F_V term, slowing down or accelerating the wave packet motion depending whether it is positive or negative. The sign of the $F_{\left[\tau,V\right]}$ is also found to determine the direction of the population transfer between the two states that are non adiabatically coupled. A Fourier analysis of the time dependence of the force allows an identification of the electronic and vibrational components in the force spectrum, as well as the electronic and vibrational periods typical of the passage of the vibronic wavepacket in the regions of non adiabatic coupling. Shifts upon isotopic substitution can be used to identify the vibrational periods in the force spectrum. The frequencies of the force spectra are also found in the spectrum of the time dependent dipole moment, which corresponds to the emitted electric field. The emission dipole can be probed directly as recently demonstrated by F. Krausz and coworkers using field resolved spectroscopy [42, 43] that allows probing electric field oscillations in real time in the THz to PHz range or by stimulated emission by a weak IR pulse as shown in ref. [18] for LiH and in ref [16] for a larger polyatomic molecule. New light sources open the way to time resolved Xray diffraction and electron diffraction which provide observables of the full density matrix.[45-49]

References

(1). Krausz, F.; Ivanov, M., 2009 *Rev. Mod. Phys. 81*, 163-234.

(2). Nisoli, M.; Decleva, P.; Calegari, F.; Palacios, A.; Martín, F., 2017 *Chem. Rev. 117*, 10760-10825.

(3). Borrego-Varillas, R.; Lucchini, M.; Nisoli, M., 2022 *Rep. Prog. Phys. 85*, 066401.

(4). Remacle, F.; Levine, R. D., 2006 *Proc. Natl. Acad. Sci. USA 103*, 6793-6798.

(5). Calegari, F.; Ayuso, D.; Trabattoni, A.; Belshaw, L.; De Camillis, S.; Anumula, S.; Frassetto, F.; Poletto, L.; Palacios, A.; Decleva, P., et al., 2014 *Science 346*, 336-339.

(6). Li, H.; Mignolet, B.; Wachter, G.; Skruszewicz, S.; Zherebtsov, S.; Süßmann, F.; Kessel, A.; Trushin, S. A.; Kling, N. G.; Kübel, M., et al., 2015 *Phys. Rev. Lett. 114*, 123004.

(7). Kraus, P. M.; Mignolet, B.; Baykusheva, D.; Rupenyan, A.; Horný, L.; Penka, E. F.; Grassi, G.; Tolstikhin, O. I.; Schneider, J.; Jensen, F., et al., 2015 *Science 350*, 790-795.

(8). Remacle, F.; Levine, R. D.; Ratner, M. A., 1998 *Chem. Phys. Lett. 285*, 25-33.

(9). Remacle, F.; Levine, R. D.; Schlag, E. W.; Weinkauf, R., 1999 *J. Phys. Chem. A 103*, 10149-10158.

(10). Cederbaum, L. S.; Zobeley, J., 1999 *Chem. Phys. Lett. 307*, 205-210.

(11). Breidbach, J.; Cederbaum, L. S., 2003 *J. Chem. Phys. 118*, 3983-3996.

(12). Kuleff, A. I.; Cederbaum, L. S., 2007 *Chem. Phys. 338*, 320-328.

(13). Muskatel, H. B.; Remacle, F.; Levine, R. D., 2009 *Phys. Scri. 80*, 048101-7.

(14). Remacle, F.; Levine, R. D., 2006 *Proc. Natl. Acad. Sci. USA 103*, 6793-6798.

(15). Remacle, F.; Nest, M.; Levine, R. D., 2007 *Phys. Rev. Lett. 99*, 183902.

(16). Valentini, A.; van den Wildenberg, S.; Remacle, F., 2020 *Phys. Chem. Chem. Phys. 22*, 22302-22313.

(17). van den Wildenberg, S.; Mignolet, B.; Levine, R. D.; Remacle, F., 2019 *J. Chem. Phys. 151*, 134310.

(18). Nikodem, A.; Levine, R. D.; Remacle, F., 2017 *Phys. Rev. A 95*, 053404.

(19). Koll, L.-M.; Maikowski, L.; Drescher, L.; Witting, T.; Vrakking, M. J. J., 2022 *Phys. Rev. Lett. 128*, 043201.

(20). Blavier, M.; Levine, R. D.; Remacle, F., 2022 *Phys. Chem. Chem. Phys. 24*, 17516-17525.

(21). Nabekawa, Y.; Midorikawa, K., 2023 *Phys. Rev. Res. 5*, 033083.

(22). Kling, M. F.; von den Hoff, P.; Znakovskaya, I.; de Vivie-Riedle, R., 2013 *Phys. Chem. Chem. Phys. 15*, 9448-9467.

(23). Kling, N. G.; Betsch, K. J.; Zohrabi, M.; Zeng, S.; Anis, F.; Ablikim, U.; Jochim, B.; Wang, Z.; Kübel, M.; Kling, M. F., et al., 2013 *Phys. Rev. Lett. 111*, 163004.

(24). Smith, F. T., 1969 *Phys. Rev. 179*, 111-123.

(25). Baer, M., *Beyond Born-Oppenheimer: Electronic Nonadiabatic Coupling Terms and Conical Intersections*. Wiley: Hoboken (NJ), 2006.

(26). Pacher, T.; Mead, C. A.; Cederbaum, L. S.; Köppel, H., 1989 *J. Chem. Phys. 91*, 7057-7062.

(27). Nijjar, P.; Jankowska, J.; Prezhdo, O. V., 2019 *J. Chem. Phys. 150*, 204124.

(28). Doltsinis, N. L., Molecular dynamics beyond the Born-Oppenheimer approximation: Mixed quantum-classical approaches. In *Computational nanoscience: Do it yourself!* ,

Grotendorst, J.; Blügel, S.; Marx, D., Eds. John von Neuman Institute for computing: Jülich, 2006.

(29). Subotnik, J. E., 2010 *J. Chem. Phys.* **132**, 134112.

(30). Jayantha, S. A.; Komarova, K. G.; Wildenberg, S. v. d.; Remacle, F.; Levine, R. D., AttoPhotoChemistry: Coherent Electronic Dynamics and Nuclear Motion. In *Attosecond Molecular Dynamics*, Vrakking, M. J. J.; Lepine, F., Eds. Royal Society of Chemistry: Cambridge, 2018; Vol. 13, pp 308-347.

(31). Ghafur, O.; Rouzee, A.; Gijsbertsen, A.; Siu, W. K.; Stolte, S.; Vrakking, M. J. J., 2009 *Nature Physics* **5**, 289-293.

(32). Kraus, P. M.; Baykusheva, D.; Wörner, H. J., 2014 *Phys. Rev. Lett.* **113**, 023001.

(33). van den Wildenberg, S.; Mignolet, B.; Levine, R. D.; Remacle, F., 2019 *J. Chem. Phys.* **151**, 134310.

(34). Frohnmeyer, T.; Baumert, T., 2000 *Appl. Phys. B* **71**, 259-266.

(35). Ergler, T.; Rudenko, A.; Feuerstein, B.; Zrost, K.; Schröter, C. D.; Moshammer, R.; Ullrich, J., 2006 *Phys. Rev. Lett.* **97**, 193001.

(36). Thumm, U.; Niederhausen, T.; Feuerstein, B., 2008 *Phys. Rev. A* **77**, 063401.

(37). Manz, J.; Pérez-Torres, J. F.; Yang, Y., 2013 *Phys. Rev. Lett.* **111**, 153004.

(38). Pérez-Torres, J. F., 2015 *Phys. Rev. A* **91**, 022510.

(39). Hermann, G.; Paulus, B.; Pérez-Torres, J. F.; Pohl, V., 2014 *Phys. Rev. A* **89**, 052504.

(40). Paulus, B.; Pérez-Torres, J. F.; Stemmle, C., 2016 *Phys. Rev. A* **94**, 053423.

(41). Komarova, K. G.; van den Wildenberg, S.; Remacle, F.; Levine, R. D., 2020 *J. Phys. B At. Mol. Opt. Phys.* **53**, 134001.

(42). Pupeza, I.; Huber, M.; Trubetskov, M.; Schweinberger, W.; Hussain, S. A.; Hofer, C.; Fritsch, K.; Poetzlberger, M.; Vamos, L.; Fill, E., et al., 2020 *Nature* **577**, 52-59.

(43). Pupeza, I.; Hofer, C.; Gerz, D.; Fürst, L.; Högner, M.; Butler, T.; Gebhardt, M.; Heuermann, T.; Gaida, C.; Maiti, K., et al., Field-resolved spectroscopy approaching ultimate detection sensitivity. Research Square: 2022.

(44). Mengxi, W.; Shaohao, C.; Seth, C.; Kenneth, J. S.; Mette, B. G., 2016 *J. Phys. B* **49**, 062003.

(45). Keefer, D.; Aleotti, F.; Rouxel, J. R.; Segatta, F.; Gu, B.; Nenov, A.; Garavelli, M.; Mukamel, S., 2021 *Proc. Natl. Acad. Sci. U.S.A* **118**, e2022037118.

(46). Rouxel, J. R.; Keefer, D.; Mukamel, S., 2021 *Struct Dyn.* **8**, 014101.

(47). Cao, J.; Wilson, K. R., 1998 *J. Phys. Chem. A* **102**, 9523-9530.

(48). Bennett, K.; Kowalewski, M.; Rouxel, J. R.; Mukamel, S., 2018 *Proc. Natl. Acad. Sci. U.S.A* **115**, 6538-6547.

(49). Yang, J.; Zhu, X.; Wolf, T. J. A.; Li, Z.; Nunes, J. P. F.; Coffee, R.; Cryan, J. P.; Gühr, M.; Hegazy, K.; Heinz, T. F., et al., 2018 *Science* **361**, 64.